Available online at www.sciencedirect.com
ScienceDirect
International Journal of Heat and Mass Transfer 51 (2008) 1582–1589
International Journal of HEAT and MASS TRANSFER
www.elsevier.com/locate/ijhmt

Isotherms and thermodynamics for the adsorption of *n*-butane on pitch based activated carbon

Bidyut Baran Saha [a,*], Anutosh Chakraborty [a], Shigeru Koyama [a], Seong-Ho Yoon [b], Isao Mochida [b], M. Kumja [c], Christopher Yap [c], Kim Choon Ng [c]

[a] *Interdisciplinary Graduate School of Engineering Sciences, Kyushu University, 6-1 Kasuga-koen, Kasuga-shi, Fukuoka 816-8580, Japan*
[b] *Institute for Materials Chemistry and Engineering, Kyushu University, 6-1 Kasuga-koen, Kasuga-shi, Fukuoka 816-8580, Japan*
[c] *Department of Mechanical Engineering, National University of Singapore, 10 Kent Ridge Crescent, Singapore 119260, Singapore*

Received 25 January 2007; received in revised form 27 June 2007
Available online 19 September 2007

Abstract

The adsorption isotherms of *n*-butane on pitch based activated carbon (type Maxsorb III) at temperatures ranging from 298 to 328 K and at different equilibrium pressures between 20 and 300 kPa have been experimentally measured by a volumetric technique. The porous properties such as, the density, Brunauer–Emmett–Teller (BET) surface area, pore size, pore volume along with pore size distribution (PSD) of Maxsorb III have been determined. The Dubinin–Astakhov (DA) adsorption isotherm model describes all of the isotherm experimental data within the acceptable error ranges. The present isotherm data are compared with other published data of activated carbon (AC)/*n*-butane and showed the superiority of the present findings in terms of uptake capacity. The isosteric heat of adsorption (ΔH_{ads}) of *n*-butane on Maxsorb III is calculated for different loading. Using the adsorption isotherms and ΔH_{ads}, the thermodynamic property maps as a function of pressure, temperature and adsorbate amount are also presented.

Keywords: Activated carbon; Adsorption; Heat of adsorption; *n*-Butane; Thermodynamic property fields

1. Introduction

The adsorption of gas or vapor is widely used in the field of gas separation [1,2], purification [3,4], adsorption chillers [5–9], cryocoolers [10] and energy storage systems [11–13]. Each of the above mentioned applications requires basic adsorption data as a function of pressure (P), temperature (T) and the amount of adsorbate (q) for understanding and predicting their performances. These data consist of adsorption isotherms, heats of adsorption and kinetics, which are required both to evaluate theories of adsorption equilibrium and to calculate energy balances for adsorption processes. Using these data, a thermodynamic property field (enthalpy, internal energy and entropy) of adsorbent–adsorbate system can be developed and analyzed for the practical interests of adsorption processes.

The porous properties of the assorted adsorbent and the adsorption characteristics of adsorbent–refrigerant pair influence directly on the operating behaviors of adsorption processes. Granular activated carbons made from coal or coconut shell have a low surface area and poor adsorption properties, so these are not suitable for industrial applications like environmental protection and medicine. Activated carbon fiber (ACF), which has a high surface area and larger adsorption capacity than granular activated carbons, is the potential candidate for adsorption process applications; however its widespread use has been limited by cost considerations and low apparent density. Pitch based activated carbons with high surface areas may offer a solution to these problems, because (i) the pitch used as raw materials is cheaper than fiber, (ii) it has a good adsorption performance, and (iii) it has high surface area,

* Corresponding author. Tel.: +81 92 583 7832; fax: +81 92 583 7833.
E-mail address: bidyutb@cm.kyushu-u.ac.jp (B.B. Saha).

0017-9310/$ - see front matter © 2007 Elsevier Ltd. All rights reserved.
doi:10.1016/j.ijheatmasstransfer.2007.07.031

Table 1
Surface area and pore volume of different activated carbons

Activated carbons	BET surface area (m^2/g)	Pore volume (cm^3/g)
Activated carbon (norit R1 extra, shape: cylindrical, raw materials: peat)	1450	0.47
Granular activated carbon (type BPL, raw material: coal)	1150	0.43
Activated carbon (raw material: crushing coconut shell)	1207	0.54
Activated carbon fiber (type A-20)	1900	1.03
Activated carbon (Kureha type)	1300	0.56
Pitch based activated carbon (type Maxsorb III)	3250	1.79

apparent density and good thermal conductivity. So these adsorbents are suitable for adsorption storage and cooling applications. The BET surface area and pore volume of different activated carbons are shown in Table 1.

It is well known that pitch based activated carbon is produced by a direct chemical activation route in which oxidative stabilized pitch derived from ethylene tar oil is reacted with potassium hydroxide under various activation conditions. Abundant oxygen-containing functional groups (C–OH, C–O–C, C=O, COOR etc.) are found to exist on its surface. On the other hand, the non-polar hydrocarbon butane consists of four carbons and ten hydrogens and generally classified as an alkane, or paraffin, where hydrogen saturates the carbon atoms via covalent single bonds. A good number of adsorption isotherms and isosteric heat of adsorption data for different adsorbates on various activated carbons are available in the literatures [14–19]. The accumulation of a data bank can be found in a handbook [20]. However, the adsorption characteristics data of pitch based activated carbon (type Maxsorb III)/*n*-butane are not available in the literature.

From the above perspectives, the motivation for this work is to investigate experimentally the porous characteristics of Maxsorb III along with the adsorption isotherms, the isosteric heat of adsorption of the Maxsorb III/*n*-butane pair. The adsorption parameters are evaluated using the DA equation. Further, the heat of adsorption data is extracted, and the thermodynamic property maps are explored for the Maxsorb III/*n*-butane pair.

2. Experimental section

2.1. Materials

The microporous adsorbent Maxsorb III manufactured by Kansai Coke and Chemicals Co. Ltd., Osaka, Japan, has been used in the present study. The porous properties such as, the BET surface area, the pore size, the pore volume, the porosity, and the skeletal density are shown in Table 2. For better appreciation of the Maxsorb III, the scanning electron microscopic (SEM) photograph for 3700 times is pictured in Fig. 1. Hence the SEM photographs show that it is closer to flake-like layers type rather than the conventional granular type. The porosity, total pore volume, average pore diameter and surface area of the activated carbon (Maxsorb III) samples are measured by the adsorption isotherm of nitrogen at 77.4 K. Samples are first treated for possible outgassing at a temperature of 473 K for 3 h and a residual pressure of 10^{-3} Pa by using an Autosorb 1 MP machine. The analysis is performed using the system's built-in data reduction software. It measures the quantity of adsorbate (gas phase) adsorbed onto or desorbed from an adsorbent surface (solid surface) at an equilibrium vapor pressure by a static volumetric method. The data are obtained by admitting or removing a known quantity of adsorbate into or out of a sample cell containing the solid adsorbent which is maintained at a constant temperature below the critical temperature of the adsorbate. As adsorption or desorption occurs, the pressure in the adsorbent–adsorbate system changes until equilibrium is established. The quantity of adsorbate gas adsorbed or desorbed at the equilibrium pressure is expressed by the difference between the amount of adsorbate gas admitted or removed and the amount required to fill the space around the void space of the assorted adsorbent. The experimental adsorption data are analyzed using the

Table 2
Porous properties of Maxsorb III

BET Surface Area (m^2/g)	3140
Micropore volume (ml/g)	1.70
Total pore volume (ml/g)	2.01
Apparent density (g/ml)	0.31
Residual heat (%)	0.1
pH (−)	4.1
Mass reduction during preparation from carbon (%)	0.8
Average particle diameter (μm)	72
Mean pore diameter (nm)	2.008

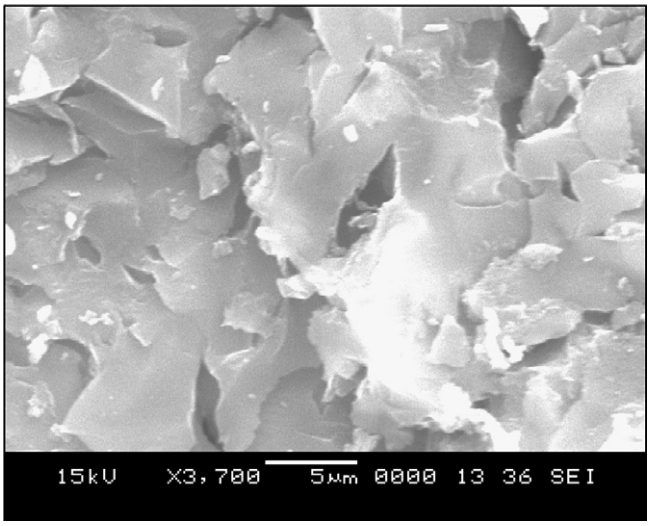

Fig. 1. Scanning electron micrographs (SEM) photos of activated carbon (type Maxsorb III) at magnifications (a) 3700 and (b) 370,000. The surface structure is observed to be flake-like structures with porous volumes embedded in between.

non-linear density functional theory (NLDFT) and pore volumes and pore size distribution (PSD) are determined. The surface area is determined by the BET method from the N_2 adsorption isotherm data. The skeletal density of the dry Maxsorb III is measured by the automated Micromeritics AccuPyc 1330 pycnometer at room temperature where the sample is regenerated at 413 K for a duration of 24 h. The mean diameter of the pore is found to be 2.008 nm which is an order higher that the molecules of the *n*-butane vapor.

2.2. Apparatus and procedure

A bench scale high pressure adsorption/desorption apparatus has been used to measure the adsorption isotherms of pure (99.998%) *n*-butane on Maxsorb III at temperatures from 298 to 328 K and pressures up to 300 kPa. Fig. 2 shows the schematic diagram of the experimental apparatus. It comprises (i) a charging tank that is made of stainless steel (SS 304) with a volume of $355.95 \pm 11.6\ \text{cm}^3$ with related piping and valves, (ii) a dosing tank that is made of SS 304 of volume $1048.0 \pm 14.6\ \text{cm}^3$ with related piping and valves, (iii) an evaporator with a volume of $200\ \text{cm}^3$, and (iv) three ball valves having volume of $1.9\ \text{cm}^3$ per valve. The charging tank is designed to have a high aspect ratio so that the adsorbent could be spread on the large flat base.

The volumes of the charging and dosing tanks are calibrated by using a calibrated standard volume ($210.9 \pm 0.2\ \text{cm}^3$) using helium gas. By measuring the pressures of the combined volumes at isothermal conditions, the volumes of both the charging and the dosing tanks are calculated using the ideal gas law. Pressures in the tanks are measured with two calibrated pressure transducer (hysteresis 0.06%) whilst the temperatures are measured with five Pt 100 Ω Class A (diameter = 1/16″) resistance temperature detectors (RTD). The RTD for the charging tank, T1 as shown in Fig. 2, is in direct contact with the Maxsorb III to give a representative adsorbent temperature. Except for the 3.175 mm vacuum adaptors used to seal the RTD probes, all other inter-connecting piping (SS 316), stainless steel vacuum fittings, and vacuum-rated stainless steel diaphragm valves are chosen to be 12.7 mm to ensure good conductance during evacuation. Isothermal condition in the two tanks is obtained by immersing them in a temperature-controlled bath (uncertainty ±0.01 K). Measurement errors caused by a temperature gradient along the piping, fittings and valves, are mitigated with a thermal jacket. All other exposed piping and fittings are also well insulated. Vacuum environment is maintained by a two-stage rotary vane vacuum pump with a pumping rate of $315 \times 10^{-6}\ \text{m}^3\ \text{s}^{-1}$. To prevent back migration of the oil mist into the apparatus, an alumina-packed fore-line trap is installed upstream of the vacuum pump. Helium with a purity of 99.9995%, is sent through a column of packed calcium sulphate before being used to purge the vacuum system. Upon evacuation, a residual gas pressure of 100 Pa is found in the apparatus.

The *n*-butane is contained in an evaporator flask which is immersed in a temperature-controlled bath. All pressure and temperature readings are continuously monitored by a calibrated data acquisition unit. The calibration of all pressure transmitters, temperature sensors, and the data logger are traceable to the National Institute of Standards and Technology (NIST) standards. In the present test facility, the major measurement bottleneck lies in the measurement of vapor pressure.

The dry mass of Maxsorb III is determined by the calibrated moisture balance of type Satorious MA40 moisture analyzer with an uncertainty of ±0.05%. The mass of the adsorbent is continuously monitored and recorded until there is no further change in the dry adsorbent mass. Maxsorb III samples typically in ranges from 2.0 to 5.124 g are introduced into the charging tank.

The dosing tank, the charging tank and all related piping systems are purged by purified but dried argon, and

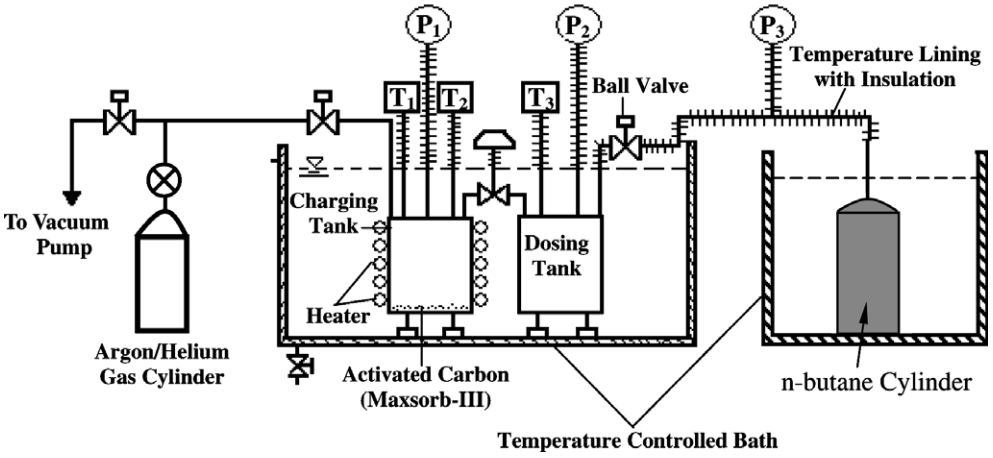

Fig. 2. Schematic diagram of the constant volume variable pressure (CVVP) test facility: *T*1, *T*2, *T*3: resistance temperature detectors or temperature sensors; P_1, P_2, P_3: pressure sensors.

evacuated. The adsorbent is again regenerated in situ at 433 K for 10 h. At the end of regeneration process, the test system is purged with helium and evacuated further to attain low vacuum conditions. The assorted adsorbent is further regenerated at 433 K for another 8 h, and the test system is evacuated again. Based on the measurements, there is no measurable interaction between the inert gas and the adsorbent, as the effect of the partial pressure of helium in the tanks is found to be small.

At first, the refrigerant *n*-butane is charged into the dosing tank. Prior to charging, the tank temperature is initially maintained at about 10 K higher than the evaporator temperature to eliminate the possibility of condensation. The evaporator is isolated from the dosing tank soon after the equilibrium pressure is achieved inside the dosing tank. Taking the effect of any residual gas, the mass of the *n*-butane is determined via the pressure and the temperature. The temperatures of the charging tank and the dosing tank are subsequently raised to the typical adsorber and desorber temperature of an adsorption cooling cycle. Once the test system reaches thermodynamic equilibrium at a desired temperature, the ball valve between the dosing and charging tank is opened, and both tanks are allowed to approach equilibrium. The temperatures of both tanks are adjusted to the desired temperature via water baths before the pressure and the temperature measurements are taken for both tanks.

With the known initial mass of dry Maxsorb III, the temperature of the test system is varied to measure the uptake of *n*-butane at a different pressure. The test system is subsequently evacuated. Maxsorb III is then regenerated, and the apparatus is purged with dried helium before *n*-butane at a given initial pressure is charged into the dosing tank to enable measurements to be made along an isotherm. Experiments are repeated at least twice for each test condition with a fresh batch of Maxsorb III to ensure repeatability and acceptable experimental uncertainty.

3. Results and discussion

3.1. N_2 adsorption data

Fig. 3 shows the nitrogen adsorption/desorption isotherm data for Maxsorb III at 77.4 K. As the adsorption experiments are run at a temperature lower than the critical capillary condensation temperature, the adsorption theory of infinite cylinder without any external surface predicts Type I adsorption isotherm for Maxsorb III, which are characterized by solid lines for adsorption and dotted lines for desorption. The Type I isotherm is given by microporous solids and is concave to the P/P_s axis and adsorption amount approaches a limiting value as $P/P_s \to 1$. Here P_s denotes the saturated pressure of the adsorbate. The very steep region at low P/P_s is due to the filling of very narrow pores and limiting uptake is dependent on the accessible micropore volume rather than on the internal surface area [21]. The breakthrough curves for Maxsorb III are completely reversible in the whole range of P/P_s i.e., they do not have any hysteresis. It is also evident from Fig. 3 that the pore filling P/P_s values for Maxsorb III are equal and are as low as 0.4.

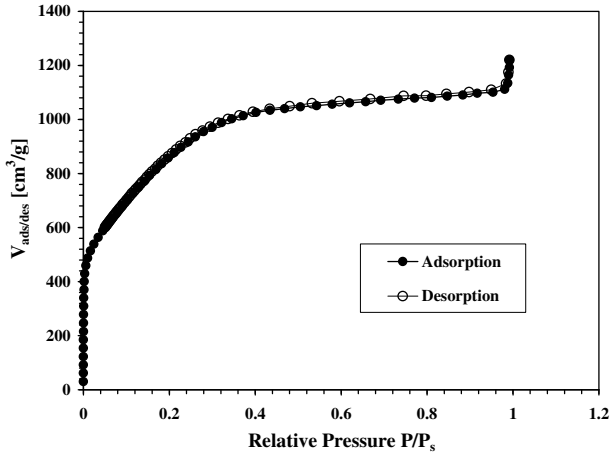

Fig. 3. Adsorption/desorption isotherm of N_2 on Maxsorb III.

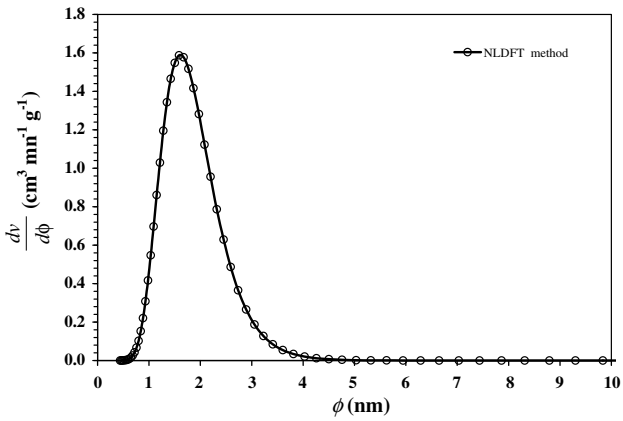

Fig. 4. The pore size distribution of Maxsorb III for NLDFT method. Here ϕ indicates the pore width and $\frac{dV}{d\phi}$ stands for the incremental pore volume.

PSD values for Maxsorb III are calculated on the basis of N_2 isotherms using the NLDFT method. To obtain a more realistic PSD appearance, the NLDFT reports (pore volume, ΔV, cm^3 g^{-1}) have been derived by normalizing the pore volume to the pore size interval (differential volume, $dV/d\phi$, cm^3 g^{-1} nm^{-1}) and the PSD results are shown in Fig. 4. The NLDFT method exhibits only one peak on the PSD curve at the pore radius of 1.67 nm and the micropore region lies between 0.1 nm and 4.4 nm. Therefore, it can be said that the Maxsorb III is highly microporous.

3.2. Adsorption isotherms

From the equilibrium measurements of *n*-butane on Maxsorb III, the measured isotherms are furnished in Table 3 and the graphical plots are shown in Fig. 5. As can be seen from Fig. 5, the isotherm of $T = 298$ K for

Table 3
Measured isotherm data for *n*-butane on Maxsorb III

Temperature (328.15 K)		Temperature (318.15 K)	
Pressure (kPa)	Uptake (kg kg^{-1})	Pressure (kPa)	Uptake (kg kg^{-1})
25.25	0.4127	20.86	0.4292
31.70	0.4586	26.86	0.4823
39.10	0.4948	33.40	0.5228
44.94	0.5215	38.95	0.5499
69.60	0.5597	62.17	0.5933
109.35	0.5916	99.44	0.6319
158.15	0.6247	148.42	0.6552
230.19	0.6609	216.49	0.6977
286.44	0.6811	270.14	0.7101
Temperature (308.15 K)		Temperature (298.15 K)	
17.33	0.4459	14.97	0.4665
22.63	0.5037	18.97	0.5228
28.50	0.5472	22.98	0.5763
32.86	0.5806	27.41	0.6094
52.65	0.6401	44.93	0.6797
89.65	0.6732	81.04	0.7096
138.98	0.6848	127.85	0.7274
203.86	0.7360	189.96	0.7824
254.14	0.75011	232.34	0.7996

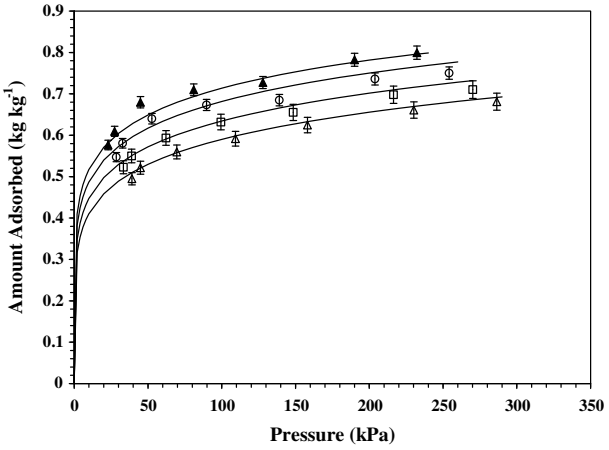

Fig. 5. Isotherm data for *n*-butane on Maxsorb III: for experimental data points with (▲)$T = 298$ K, (○) $T = 308$ K, (□) $T = 318$ K, and (△) $T = 328$ K; for computed data points with solid lines for D–A equation.

Maxsorb III-*n*-butane pair exhibits signs of monolayer saturation at high pressure. For design purposes, the experimental data should be marched with an analytical expression that includes adjustable parameters as a function of pressure and temperature. The Maxsorb III is a highly microporous material and its pore size distribution is wide, which ranges from 0.4 to 3 nm. Therefore, Maxsorb III is considered to be a heterogeneous adsorbent. For the adsorption on carbon based heterogeneous adsorbents, the Dubinin–Astakhov isotherm equation [22,23] is found suitable and hence the DA equation is used to correlate the experimental isotherm data. The DA equation can be written as

$$q = q_{\mathrm{m}} \exp\left[-\left\{\frac{RT}{E}\ln\left(\frac{P_{\mathrm{s}}}{P}\right)\right\}^{n}\right] \quad (1)$$

where q is the adsorbed quantity of adsorbate by the adsorbent under equilibrium conditions, q_{m} denotes the monolayer capacity, P the equilibrium pressure of the adsorbate in gas phase, T the equilibrium temperature of gas phase adsorbate, R the universal gas constant. The parameter, E denotes the activation energy and n is an exponential constant usually varies between 1 and 3 [24,25]. The exponential constant n depends on the width of the distribution curve of adsorption activation energy. By using Curve-Expert 1.3 software, we have regressed the experimental data and the parameters q_{m}, E, n of Eq. (1) are found to be 0.8 kg kg^{-1}), 300 kJ kg^{-1}) and 1.05, respectively.

It is instructive to compare the present isotherm data with the published references [14,18,26]. The activated carbon used by Ref. [14] is of granular type, whereas that used by ref [18] is Brazilian coconut shell, and that used by ref [26] is known as Kureha type activated carbon. Fig. 6 presents the isotherm comparisons of the present data with those of the above mentioned activated carbon/*n*-butane systems at 298 K. It is evident from Fig. 6, that the adsorption uptake of *n*-butane on Maxsorb III is significantly higher than those obtained by other researchers. On the other hand, the adsorption kinetics of Maxsorb III/*n*-butane system has been great interest in the field of transient adsorption cooling sector. The amount of adsorbate (*n*-butane) uptake on adsorbent (pitch based activated carbon of type Maxsorb III) as a function of time is shown in Fig. 7. In most cases the *n*-butane adsorption is very fast and occurs within few minutes and it takes about twenty five minutes to reach the thermal equilibrium. The usual encountered equilibrium times are captured between 100 and 300 s. It is noted that the most unfavorable kinetic condition appears at low temperatures and low pressures.

3.3. Adsorption thermodynamics

From the experimentally measured adsorption isotherms, the isosteric heat of adsorption (ΔH_{ads}) as a func-

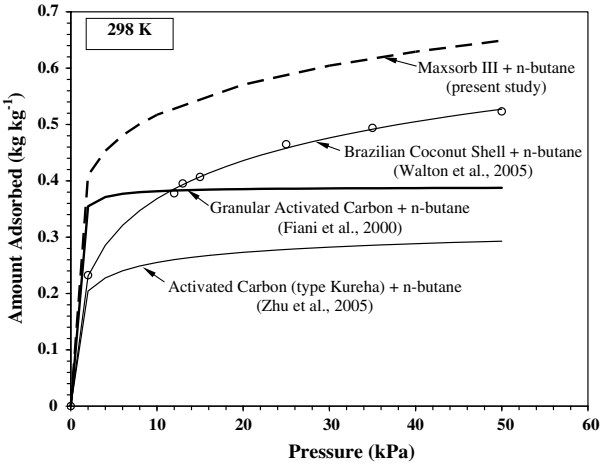

Fig. 6. Comparison of isotherm data for Maxsorb III/*n*-butane and different activated carbons + *n*-butane systems.

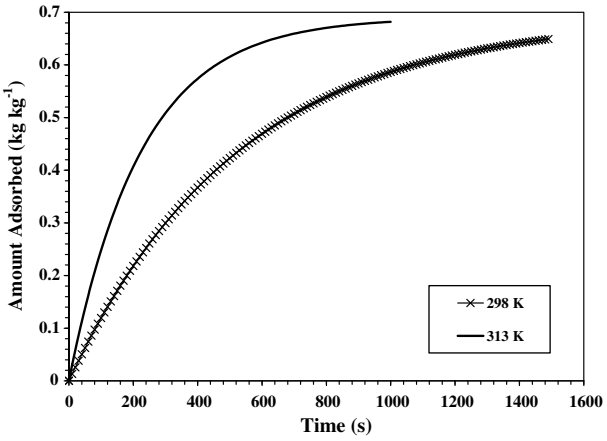

Fig. 7. The kinetics of *n*-butane on Maxsorb III.

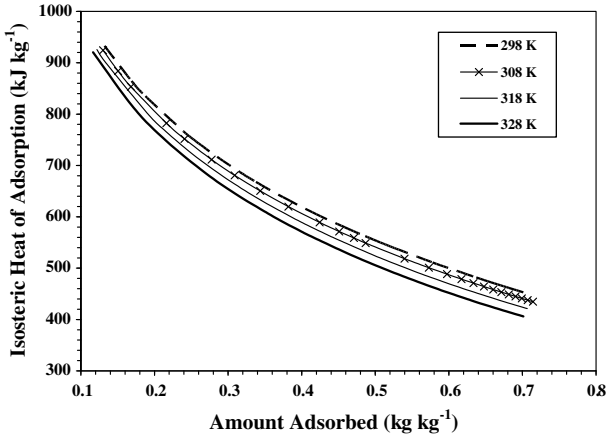

Fig. 8. Isosteric heat of adsorption data for *n*-butane onto Maxsorb III for uptake at (a) $T = 298$ K, (b) $T = 308$ K, (c) $T = 318$ K, and (d) $T = 328$ K.

tion of loading (q) can be calculated by the following equation [27]

$$\Delta H_{\text{ads}} = RT^2 \left[\left(\frac{\partial(\ln P)}{\partial T} \right)_{m_a} \right] + T v_g \frac{dP}{dT}(P,T), \tag{2}$$

where the first term of the right hand side indicates the conventional form of the isosteric heat of adsorption derived from the Clausius–Clapeyron equation and the second term defines the behavior of adsorbed mass with respect to both the pressure and the temperature changes during an adsorbate uptake, which occurs due to the non-ideality of the gaseous phase. Using the DA equation, Eq. (2) can be written as,

$$\Delta H_{\text{ads}} = h_{\text{fg}} + E \ln \left(\frac{q^*}{q} \right)^{\frac{1}{n}} + T v_g \frac{dP}{dT}(P,T) \tag{3}$$

The isosteric heat of adsorption (ΔH_{ads}) for *n*-butane on Maxsorb III as a function of surface loading and temperature are shown in Fig. 8. From Fig. 8, one can observe that ΔH_{ads} decreases with increasing loading. The Maxsorb III consists mainly of micropores with different widths and *n*-butane adsorbs rapidly onto sites of high energy, and as adsorption progresses, molecules then adsorb onto sites of decreasing energy. The *n*-butane molecules first penetrate into narrower pores, resulting in a stronger interaction between the adsorbate and the adsorbent. This implies a higher value of ΔH_{ads} at lower loadings. After completely filling the smaller pores, *n*-butane molecules are gradually accommodated in larger pores, in which the adsorption affinity becomes weaker. Therefore, a monotonic decrease in the ΔH_{ads} as a function of loading is observed.

The extensive thermodynamic properties such as enthalpy (h) and entropy (s) of an adsorbent–adsorbate system have been developed from the rigor of classical thermodynamics and these are written as

$$h = c_{p,ac} \cdot \int_{T_0}^{T} dT + q \int_{T_0}^{T} \left[c_{p,g}(P,T) + \frac{\Delta H_{\text{ads}}}{T} - \frac{\Delta H_{\text{ads}}}{v_g} \frac{\partial v_g}{\partial T} \right] dT + \int_0^q \left[h_g(P,T) - \Delta H_{\text{ads}} \right] dq + \int_{P_0}^{P} v_{ac}\, dP \tag{4}$$

and

$$s = c_{p,ac} \int_{T_0}^{T} \frac{dT}{T} + q \times \int_{T_0}^{T} \left[c_{p,g}(P,T) + \frac{\Delta H_{\text{ads}}}{T} - \frac{\Delta H_{\text{ads}}}{v_g} \frac{\partial v_g}{\partial T} \right] \frac{dT}{T} + \int_0^q \left[s_g(P,T) - \frac{\Delta H_{\text{ads}}}{T} \right] dq, \tag{5}$$

where $c_{p,ac}$ is the specific heat capacity of the Maxsorb III [28], v_g indicates the specific volume of the gaseous phase.

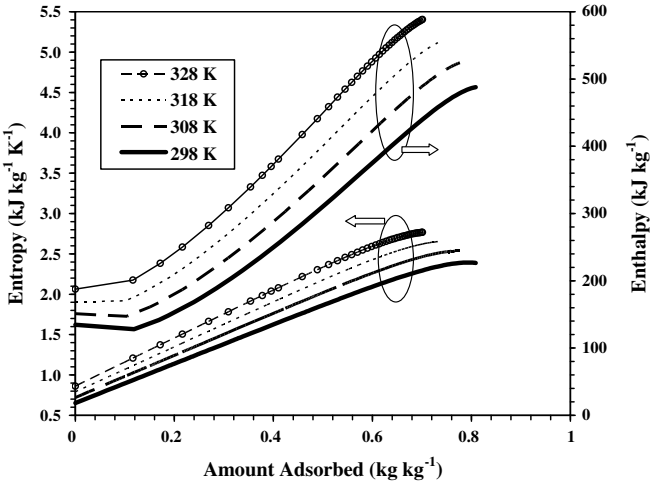

Fig. 9. Temperature–entropy and temperature–enthalpy maps for *n*-butane onto Maxsorb III for different amount of adsorbate. Here the reference temperature $T_0 = 135$ K (triple point value) and the reference pressure $P_0 = 0$ kPa are considered for calculation.

Subscripts "g" and "0" indicate the gaseous phase and the reference value in these above equations. Using the experimentally measured adsorption isotherm data and the isosteric heat of adsorption, the extensive properties h and s are calculated as a function of adsorption uptake q and these are shown in Fig. 9. From Fig. 9, one could observe that the entropy (s) of an adsorbent–adsorbate system is an increasing function of uptake (q) and temperature (T). Hence, s goes through a maximum value against uptake or surface coverage and the curves approximately approach a constant value when the filling of n-butane adsorbate on Maxsorb III becomes weaker. Such curves represent the characteristics of heterogeneous surfaces. On the other hand, the enthalpy (h) also increases with surface coverage, reaches a maximum and approaches to constant.

4. Conclusions

The isothermal characteristics and the porous properties of Maxsorb III are determined from the nitrogen adsorption isotherms, which are followed by equilibrium adsorption isotherm of Maxsorb III/n-butane pair. As of the nitrogen adsorption/desorption isotherms at 77.4 K, Maxsorb III has no hysteresis and can be characterized by Type I isotherm. The porous property data show that the BET surface area and micropore volume of Maxsorb III are 3140 $m^2 g^{-1}$ and 1.70 ml g^{-1}, respectively. The derived monolayer capacity of Maxsorb III-n-butane pair has been measured 0.8 kg kg^{-1}. We have found that the isosteric heat of adsorption varies from 406 to 975 kJ kg^{-1} depending on the adsorbate loading. The thermodynamic property fields such as the entropy (s), the enthalpy (h) of Maxsorb III/n-butane systems are presented in terms of pressure, temperature and the amount of adsorbate. The information of isotherms, kinetics and thermodynamics for Maxsorb III/n-butane system has immense importance as it affects directly the computation of the energy and entropy balances of the adsorbed phase, which in turn is employed for the design and analysis adsorption processes in cooling applications.

Acknowledgements

This work was financially supported by the Ministry of Education, Culture, Sports, Science and Technology (MEXT), Japan, "Science and Technology Project", Project No. 18650205.

References

[1] G. Arora, S.L. Sandler, Mass transport of O_2 and N_2 in nanoporous carbon (C168 Schwarzite) using a quantum mechanical force field and molecular dynamics simulations, Langmuir 22 (10) (2006) 4620–4628.
[2] X. Liu, J. Li, L. Zhou, D. Huang, Y. Zhou, Adsorption of CO_2, CH_4 and N_2 on ordered mesoporous silica molecular sieve, Chem. Phys. Lett. 415 (4-6) (2005) 198–201.
[3] A.N. Fedorov, Investigation and improvement of cryogenic adsorption purification of argon from oxygen, Gas Separat. Purificat. 9 (2) (1995) 137–145.
[4] J.G. Jee, M.B. Kim, C.H. Lee, Pressure swing adsorption processes to purify oxygen using a carbon molecular sieve, Chem. Eng. Sci. 60 (3) (2005) 869–882.
[5] B.B. Saha, A. Akisawa, T. Kashiwagi, Silica gel water advanced adsorption refrigeration cycle, Energy 22 (4) (1997) 437–447.
[6] B.B. Saha, K.C.A. Alam, A. Akisawa, T. Kashiwagi, K.C. Ng, H.T. Chua, Two-stage non-regenerative silica gel–water adsorption refrigeration cycle, Proceedings of the ASME Advanced Energy Systems Division, Orlando 40 (2000) 65–69.
[7] B.B. Saha, S. Koyama, J.B. Lee, K. Kuwahara, K.C.A. Alam, Y. Hamamoto, A. Akisawa, T. Kashiwagi, Performance evaluation of a low-temperature waste heat driven multi-bed adsorption chiller, Int J Multiphase Flow 29 (8) (2003) 1249–1263.
[8] B.B. Saha, A. Chakraborty, S. Koyama, K.C. Ng, M.A. Sai, Performance modelling of an electro-adsorption chiller, Philosop. Magaz. 86 (23) (2006) 3613–3632.
[9] B.B. Saha, I.I. El-Sharkawy, S. Koyama, J.B. Lee, K. Kuwahara, Waste heat driven multi-bed adsorption chiller: heat exchangers overall thermal conductance on chiller performance, Heat Transfer Eng. 27 (5) (2006) 80–87.
[10] R. Baby, M.J. Prakash, Improving the performance of an active carbon–nitrogen adsorption cryocooler by thermal regeneration, Carbon 43 (11) (2005) 2338–2343.
[11] L. Schlapbach, A. Züttel, Hydrogen-storage materials for mobile applications, Nature 414 (2001) 353–358.
[12] S.K. Bhatia, A.L. Myers, Optimum conditions for adsorptive storage, Langmuir 22 (4) (2006) 1688–1700.
[13] A. Feaver, G. Cao, Activated carbon cryogels for low pressure methane storage, Carbon 44 (3) (2006) 590–593.
[14] E. Fiani, L. Perier-Cambry, G. Thomas, Non-isothermal modelling of hydrocarbon adsorption on a granulated active carbon, J. Therm. Anal. Calorimet. 60 (2000) 557–570.
[15] Y. He, J.H. Yun, N.A. Seaton, Adsorption equilibrium of binary methane/ethane mixtures in BPL activated carbon: isotherms and calorimetric heats of adsorption, Langmuir 20 (16) (2004) 6668–6678.
[16] W. Zhu, J.C. Groen, F. Kapteijn, J.A. Moulyn, Adsorbtion of butane isomers and SF6 on Kureha activated carbon: 1. Equilibrium, Langmuir 20 (13) (2004) 5277–5284.
[17] C. Garnier, T. Gorner, A. Razafitianamaharavo, F. Villie'ras, Investigation of activated carbon surface heterogeneity by argon and nitrogen low-pressure quasi-equilibrium volummetry, Langmuir 21 (7) (2005) 2838–2846.
[18] K.S. Walton, C.L. Cavalcante Jr., M.D. Levan, Adsorption equilibrium of alkanes on a high surface area activated carbon prepared from Brazilian coconut shells, Adsorption 11 (2005) 107–111.
[19] I.I. El-Sharkawy, B.B. Saha, S. Koyama, K.C. Ng, A study on the kinetics of ethanol-activated carbon fiber: theory and experiments, Int. J. Heat Mass Transfer 49 (2006) 3104–3110.
[20] D.P. Valenzuela, A.L. Myers, Adsorption Equilibrium Data Handbook, Prentice Hall, Englewood Cliffs., USA, 1989.
[21] Z. Ryu, J. Zheng, M. Wang, B. Zhang, Characterization of pore size distributions on carbonaceous adsorbents by DFT, Carbon 37 (8) (1999) 1257–1264.
[22] M.M. Dubinin, V.A. Astakhov, L.V. Radushkevich, D.A. Cadenhead, J.F. Danielli, M.D. Rosenberg, Physical Adsorption of Gases and Vapors in Micropores, Progress and Membrane Science, Academic Press, New York, 1975, pp. 1–70.
[23] B.S. Akkimaradi, M. Prasad, P. Dutta, K. Srinivasan, Adsorption of 1,1,1,2-tetrafluoroethane on activated charcoal, J. Chem. Eng. Data 46 (2) (2001) 417–422.
[24] R.Z. Wang, Q.B. Wang, Adsorption mechanism and improvements of the adsorption equation for adsorption refrigeration pairs, Int. J. Energ. Res. 23 (1999) 887–898.

[25] I.I. El-Sharkawy, K. Kuwahara, B.B. Saha, S. Koyama, K.C. Ng, Experimental investigation on adsorption of ethanol onto activated carbon fibers for possible application in adsorption cooling system, Appl. Therm. Eng. 26 (8–9) (2006) 859–865.
[26] W. Zhu, F. Kapteijn, J.C. Groen, J.A. Moulijn, Adsorption on Kureha activated carbon: isotherms and kinetics, Adsorption 11 (Suppl. 1) (2005) 637–641.
[27] A. Chakraborty, B.B. Saha, S. Koyama, K.C. Ng, On the thermodynamic modeling of the isosteric heat of adsorption and comparison with experiments, Appl. Phys. Lett. 89 (2006) 171901.
[28] A. Chakraborty, B.B. Saha, S. Koyama, K.C. Ng, The specific heat capacity of a Single component adsorbent–adsorbate system, Appl. Phys. Lett. 90 (2007) 171902.